Hafnium coordination vitrimer based on carboxylate exchange: synthesis, properties, and mechanistic investigations on the [Hf 6 O 4 (OH) 4 (O 2 CMe) 12] 2 model compound

Meenu Murali, Dimitri Berne, Jean-claude Daran, Christian Bijani, Eric Manoury, Eric Leclerc, Vincent Ladmiral, Sylvain Caillol, Christine Joly-Duhamel, Rinaldo Poli

Hafnium coordination vitrimer based on carboxylate exchange: synthesis, properties, and mechanistic investigations on the $[Hf_6O_4(OH)_4(O_2CMe)_{12}]_2$ model compound

Meenu Murali,[a] Dimitri Berne,[b] Jean-Claude Daran,[a] Christian Bijani[a], Eric Manoury,[a] Eric Leclerc,[b] Sylvain Caillol,[b] Vincent Ladmiral,[b] Christine Joly-Duhamel,*[b] Rinaldo Poli*[a,c]

[a] Dr. M. Murali, Dr. J.-C. Daran, Dr. C. Bijani, Dr. E. Manoury, Prof. R. Poli
LCC (Laboratoire de Chimie de Coordination)
CNRS, UPS, INP, Université de Toulouse
205 Route de Narbonne, 31077 Toulouse, France
E-mail: rinaldo.poli@lcc-toulouse.fr

[b] Dr. D. Berne, Dr. C. Joly-Duhamel, Dr. V. Ladmiral
ICGM
CNRS, Univ Montpellier, ENSCM
1919 Route de Mende, 34090 Montpellier, France

[c] Prof. R. Poli
Institut Universitaire de France,
1 rue Descartes, 75231 Paris, France

Supporting information for this article is given via a link at the end of the document.

Abstract: A hafnium-based coordination vitrimer (Hf-CooAN-10) has been prepared by carboxylate ligand exchange from $[Hf_6O_4(OH)_4(O_2CMe)_{12}]_2$ and poly-((ethylhexyl methacylate)-*co*-(carboxyethyl acrylate)) (M_n = 14.4 kg mol^{-1}, Đ = 2.2, 90:10 comonomer molar ratio), using a 10% molar Hf loading with respect to the polymer maximum crosslinking capacity. The material shows high insoluble fraction and expected properties for a 3D network and has been reshaped three times at 50 °C under a 3-ton pressure without significant property alteration. The Hf-CooAN-10 thermomechanical and rheological properties are very similar to those previously reported for the analogous Zr-CooAN-10. The associative nature of carboxylate exchange between the $[Hf_6O_4(OH)_4(O_2CR)_{12}]$ crosslinks and the polymer matrix free -COOH functions is suggested by parallel ^{1}H NMR line-broadening kinetic investigations of acetate exchange in the $[Hf_6O_4(OH)_4(O_2CMe)_{12}]_2$ precursor with free MeCOOH, the rate of which has a zero-order dependence on [MeCOOH], and by DFT calculations on a $[Hf(\mu\text{-}O_2CMe)(O_2CMe)_2(OH)(H_2O)]_2$ model. The results of these investigations, including the activation parameters for the exchange of both chelating and bridging ligands, are very similar to those of the previously investigated zirconium system and suggest partial acetate dissociation assisted by H-bond formation with a (μ_3-OH) ligand as the rate-determining step, followed by acid coordination and intramolecular proton transfer.

Introduction

The area of polymer-based moldable materials has experienced a quantum leap with the introduction of dynamic crosslinks, leading to Covalent Adaptable Networks (CANs),[1] which blur the distinction of thermoplastics and thermosets. The degenerate exchange reactions leading to the crosslink migration in CANs may have either a dissociative or an associative character. While a loss of connectivity at high temperature occurs in the first case, associative CANs have a T-independent crosslink density and have also been named “vitrimers”,[2] because their rheology is similar to that of vitreous silica.[3]

Polymer adaptable networks may also be based on the migration of non-covalent crosslinks. In this respect, coordination chemistry has played a significant role, yielding a rather broad and growing family of Coordination Adaptable Networks (CooANs), also known as “self-healing metallopolymers”.[4] In addition to reshaping under generally milder conditions than CANs, CooANs also benefit from the intrinsic properties of the metallic crosslink (optical, magnetic, catalytic, *etc.*), thus leading to many possible applications. If the exchange reaction has an associative character, these materials may also be named “coordination vitrimers”. Several types of ligands have so far been used, *e.g.* imidazoles, pyridines, catecholates, thiolates and carboxylates. Neutral (L-type) two electron donors such as imidazoles and pyridines may readily undergo dissociative exchange, whereas a dissociative process for anionic (X-type) ligands requires charge separation, which may be difficult in a low-permittivity organic polymer matrix. On the other hand, an associative exchange is conceivable with the assistance of a proton (*i.e.* a polymer-linked XH function). However, most investigations carried out so far have focused on the mechanical and rheological behavior and have given only limited attention to the intimate mechanism of the ligand exchange responsible for crosslink migration.[5]

We have recently reported CooANs based on a carboxylic acid-functionalized polymethacrylate matrix, crosslinked by $[Zr_6O_4(OH)_4]^{12+}$.[6] This zirconium oxo-hydroxo cluster core is commonly found in neutral $[Zr_6O_4(OH)_4(O_2CR)_{12}]_n$ complexes (n = 1 or 2)[7] and in metal-organic frameworks.[8] The molecular complexes have been shown to adopt one of three possible structures, depending on the R nature and the crystallization conditions (Figure 1, M = Zr). These structures are interchangeable at high temperature[9] and the carboxylate ligands are readily exchanged with external R’COOH under mild

conditions.[7d, 10] Thus, all three possible geometries shown in Figure 1 may be present in the Zr-CooANs and the crosslink migration may occur by exchange of both chelating and bridging carboxylate ligands.

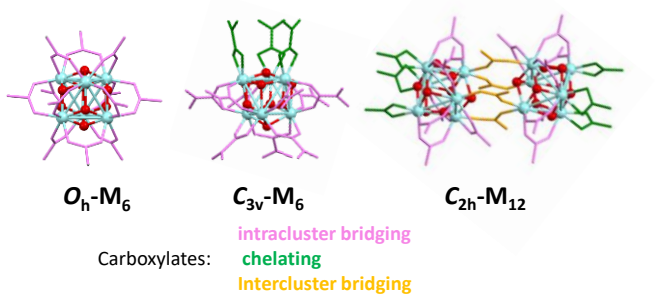

Figure 1. Topologies of $[M_6O_4(OH)_4(O_2CR)_{12}]_n$ clusters (M = Zr, Hf; n = 1 or 2).

We have also reported a detailed kinetico-mechanistic study, based on variable-temperature and variable-concentration ^{1}H NMR spectra, on the model $[Zr_6O_4(OH)_4(O_2CMe)_{12}]_2$ compound (C_{2h}-Zr_{12} structure of Figure 1), which demonstrated an operationally associative exchange mechanism for the chelating acetates and for most of the intracluster-bridging acetates.[11] The rate-determining step, however, consists of partial acetate dissociation with assistance of a neighboring bridging hydroxide ligand, which provides a stabilizing H-bonding interaction (Scheme 1).

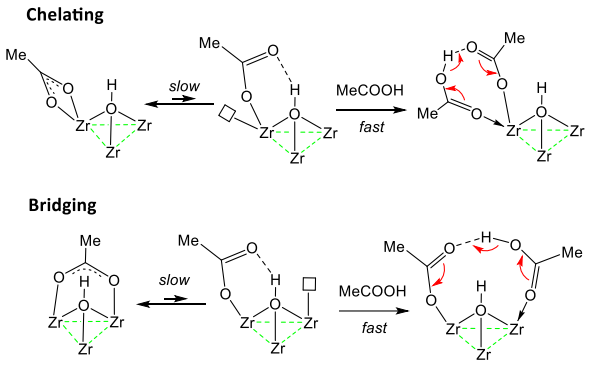

Scheme 1. Operationally associative exchange with a rate-determining partial dissociation, assisted by a neighboring OH ligand, for chelating and bridging acetates in compound $[Zr_6O_4(OH)_4(O_2CR)_{12}]$.[11]

Zirconium and hafnium in the oxidation state IV have very similar ionic radii and chemical behavior, to the point of being considered as the two most similar ions in the periodic table. Minor differences, however, are exploited to accomplish their difficult separation.[12] A few carboxylate derivatives containing the $[Hf_6O_4(OH)_4]^{12+}$ core[7d, 13] and a few MOFs[8c, 14] based on the $[Hf_6O_4(OH)_4]^{12+}$ core as crosslinker have been developed, though the chemistry of oxo-hydroxo hafnium(IV) is generally much less developed than that of zirconium(IV). In terms of carboxylate exchange, both C_{2h}-symmetric $[M_6O_4(OH)_4(O_2CMe)_{12}]_2$ clusters (M = Zr, Hf) were shown to undergo the same conversion to an M_6 structure by substitution with methyl heptanoate.[9]

The present contribution presents the synthesis and the rheological and reshaping properties of the first hafnium-based CooAN, and a kinetico-mechanistic investigation of carboxylate exchange on the $[Hf_6O_4(OH)_4(O_2CMe)_{12}]_2$ compound. The primary goal of this investigation was a direct comparison between the two homologous metals (Zr and Hf) in terms of the exchange kinetics in the model compounds and mechanical/rheological properties of the adaptable networks.

Results and Discussion

New synthesis of $[Hf_6O_4(OH)_4(O_2CMe)_{12}]_2$

In order to assess the effect of the Hf/Zr substitution on the properties, the material was synthesized by the same strategy (Scheme 2), namely carboxylate exchange from $[Hf_6O_4(OH)_4(O_2CMe)_{12}]_2$ and the same COOH-functionalized polymer.[15] The $[Hf_6O_4(OH)_4(O_2CMe)_{12}]_2$ compound was previously obtained, like the Zr homologue, from $Hf(O^tBu)_4$ and acetic acid in CH_2Cl_2.[7d] Given the significantly higher cost of the commercially available $Hf(O^tBu)_4$ than $Zr(O^tBu)_4$, a new synthetic approach was first considered. The related $[Zr_6O_4(OH)_4(O_2CMe)_{12}]_2$ cluster was also synthesized by Dietzel *et al.* from $ZrOCl_2{\cdot}8H_2O$ in the presence of excess acetic acid in DMF at 110 °C.[16]. Application of this method to the commercially available and comparatively inexpensive $HfOCl_2{\cdot}8H_2O$ indeed produced $[Hf_6O_4(OH)_4(O_2CMe)_{12}]_2$.

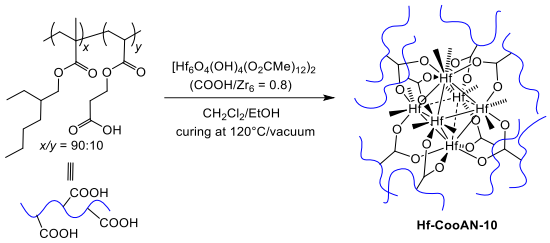

Scheme 2. Synthesis of Hg-CooAN-10. The drawn crosslink structure for the product is one of several possibilities (one or more polymer-bound carboxylates may be replaced by an acetate ligand). For clarity, the μ_3-O and μ_3-OH ligands are omitted and 8 ligands in the equatorial plane are unspecified.

Single crystals were obtained and analyzed by X-ray diffraction. The compound crystallized with interstitial acetic acid and formic acid molecules, the latter presumably deriving from hydrolysis of the DMF solvent used in the synthesis. In this respect, the $[Zr_6O_4(OH)_4(O_2CMe)_{12}]_2$ compound prepared under the same conditions also crystallized with acetic and formic acid molecules and the two structures are isomorphous.[16] A view of the $[Hf_6O_4(OH)_4(O_2CMe)_{12}]_2$ molecule is shown in Figure 2 and an additional view highlighting the H-bonding interactions of the metal complex with the interstitial acids is available in Figure S1. The structure of the $[Hf_6O_4(OH)_4(O_2CMe)_{12}]_2$ molecule is essentially identical to that reported by Schubert *et al.* for the same compound[7d] and to those of the corresponding Zr cluster.[7d, 16] A comparison of the most significant parameters for the $[Hf_6O_4(OH)_4]^{12+}$ core in the two Hf structures is available in Table S2.

The presence of formic acid along with acetic acid was considered to potentially affect the properties of the materials, as well as the kinetics of the acetate exchange reactions (of importance in the next section). Thus, for comparative purposes, the starting material prepared from $Hf(O^tBu)_4$, which contains

acetic acid and dichloromethane as co-crystallized molecules, was eventually used.[7d]

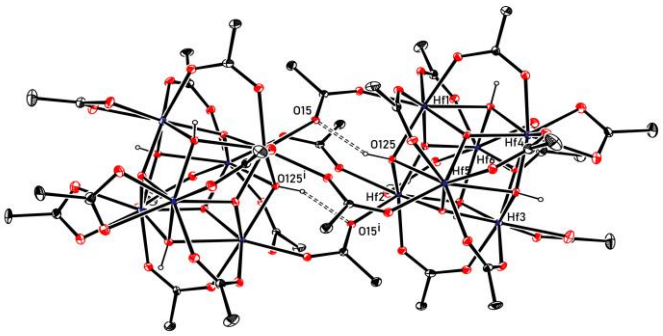

Figure 2. ORTEP view of the $[Hf_6O_4(OH)_4(O_2CMe)_{12}]_2$ molecule. All H atoms, except those of the μ_3-OH ligands, and the interstitial acetic and formic acid molecules are omitted for clarity. The ellipsoids are drawn at the 30% probability level.

Preparation of Hf-CooAN-10

For the previously published Zr-CooAN materials, model studies on well-defined diacid linkers with flexible alkyl chains (*i.e.* adipic and sebacic acid) showed that only eight of the twelve acetates in $[Zr_6O_4(OH)_4(O_2CMe)_{12}]$ can be exchanged, even in the presence of excess linker.[6] In the resulting $[Zr_6O_4(OH)_4(O_2CR)_8(XL)_4]$ products where R is the organic linker, the (XL) ligands may be either residual acetates or $(OH)(H_2O)$ combinations. Incidentally, this stoichiometry is also witnessed in several MOFs with alkyl-based diacid linkers.[17] Thus, in the previous investigation on the Zr-CooAN materials, a COOH/Zr_6 stoichiometry of 8:1 was assumed to correspond to the ideal fully crosslinked polymer (no residual free -COOH in the polymer matrix). Flexible and reshapable Zr-CooAN-x materials (x = percent of polymer-linked -COOH functions coordinated to the Zr_6 crosslinks), were obtained for x = 5, 10, 15, 20, 25, 30 and 50, whereas a brittle and non-reshapable material was obtained for x = 100.[6] For hafnium, the same assumption was made (COOH/Zr_6 stoichiometry of 8:1 for a fully crosslinked network). The present study was limited to the synthesis of the Hf-CooAN-10 material (*i.e.* COOH/Hf_6 = 0.8), since the most thoroughly investigated Zr-CooAN-x material in terms of spectroscopic, mechanical and rheological properties and reshaping behavior was the material with x = 10.

Hf-CooAN-10 was successfully prepared according to the same protocol used for Zr-CooAN-10,[6] mixing an ethanol solution of $[Hf_6O_4(OH)_4(O_2CMe)_{12}]_2$ with a solution of the polymer followed by curing at 120°C under vacuum to remove the CH_3COOH produced by the exchange, except that the polymer was dissolved in dichloromethane, rather than in toluene. Indeed, when the material was made using a toluene solution of the polymer, although having the same aspect as a flexible transparent solid, the FTIR spectrum revealed only a small band attributable to coordinated carboxylates (Figure S2). Using dichloromethane, on the other hand, the absorption band of the Hf-coordinated carboxylate in the product (observed at 1601 cm^{-1}) had a relative intensity (*versus* the normalized band of the polymer ester groups at 1705 cm^{-1}) approximately identical to that of the 1593 cm^{-1} band measured for the corresponding Zr-CooAN-10 material (Figure 3), suggesting a similar extent of polymer crosslinking. The more successful crosslinking from the dichloromethane/ethanol mixture is probably related to solubility issues. Indeed, the Hf precursor is less toluene soluble (*ca.* 8 mg/mL) than the Zr precursor (>10 mg/mL) and probably precipitates in the form of nanocrystals upon addition of the polymer solution, preventing the exchange reaction to occur to a significant extent. The dichloromethane/ethanol mixture, on the other hand, appears to be a better solvent for both reaction components.

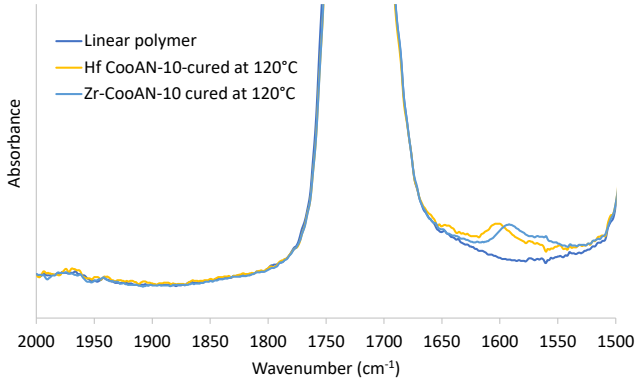

Figure 3. Comparison of the Hf-CooAN-10 FTIR spectrum with those of the Zr-CooAN-10 material and of the metal-free polymer.

Characterization of Hf-CooAN-10

The Hf-CooAN-10 material swells without complete dissolution at room temperature in THF, which is a good solvent for the linear polymer, confirming its crosslinked nature. The swelling ratio (15.0 ± 3.3) and the insoluble fraction (0.58 ± 0.02) are similar to those of the corresponding Zr-CooAN-10 (12.7 ± 0.4 and 0.73 ± 0.02, respectively),[6] though the slight difference suggests a slightly less efficient crosslinking for the Hf material. The TGA of the Hf-CooAN-10 shows an onset decomposition temperature similar to those of Zn-CooAN-10 and metal-free polymer (ca. 220 °C), but it subsequently decomposes faster than Zr-CooAN-10, though more slowly than the metal-free polymer (Figure S4).

Frequency sweep and creep-recovery tests were carried out to evaluate the Hf-CooAN-10 dynamic behavior. In the case of crosslinked linear polymers, viscosity is typically determined from creep/recovery experiments rather than from stress relaxation. Indeed, the observed immediate and fast decrease of stress at the beginning of the stress relaxation experiments was shown to interfere with the derivation of the characteristic relaxation time in those cases.[18] Conversely, the material viscosity can be precisely determined from the compliance ($J(t)=\gamma(t)/\sigma_0$), which is inversely proportional to the viscosity ($J(t)=t/\eta_0+J_0$), obtained from the linear region of the creep/recovery analysis. The J_0 parameters is the steady-state linear recoverable compliance (Figure S5).

An Arrhenius-type behavior of the viscosity as a function of temperature, as is typical of vitrimers, was observed (Figure 4), consistent with (but not proving) the associative character of the crosslink migration. Indeed, an Arrhenius-type behavior has also been highlighted for several dissociative CANs.[19] For this reason, a more detailed mechanistic investigation of carboxylate exchange on a molecular model of the Hf-CooAN-10 crosslink was also carried out (*vide infra*). The Hf-CooAN-10 material exhibited higher viscosities than the Zr-CooAN-10 analogue in the

studied temperature range, suggesting faster exchange for the Zr cluster. However, the flow activation energies are not significantly dependent of the metal nature (86.6 ±5.9 kJ mol^{-1} for Hf-CooAN-10 *vs.* 92.9 ±3.6 kJ mol^{-1} for Zr-CooAN-10).

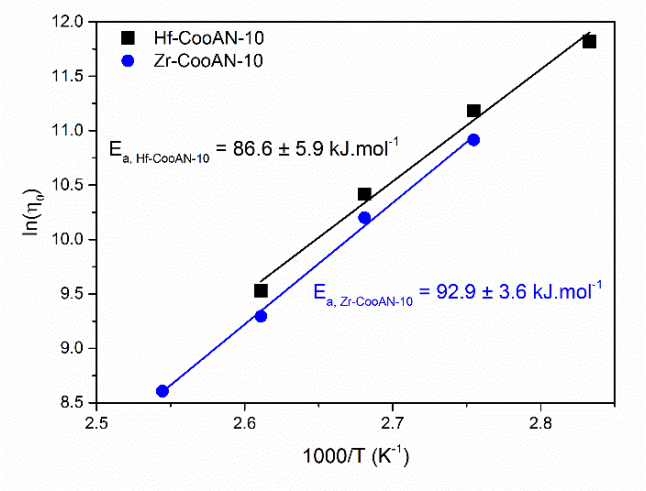

Figure 4. Comparison of the Arrhenius plots of the T-dependent viscosity determined from the compliance linear region for Hf-CooAN-10 and Zr-CooAN-10.

Dynamic properties are also revealed by frequency analyses, in particularly the crossing of G' and G'' is characteristic of the material relaxation. The Hf-CooAN-10 and Zr-CooAn-10 materials show the G'/G" crossing at approximately the same frequency (Figure S6) in the measurements carried out at 160 °C, indicating a similar relaxation behavior. This result agrees with the creep results (Figure S5), collectively showing a relatively small viscosity difference between the two materials.

Based on these rheological observations, it is not surprising that the temperature, pressure and time needed to reprocess Hf-CooAN-10 are similar to those used to reprocess Zr-CooAN-10 (50 °C in 30 minutes under 3 tons). These two materials could be reprocessed for three cycles without visible alteration of the Young modulus and of the stress/strain at break measured by tensile tests (Table 1). Frequency sweep (Figure S7) and DMA (Figure S8) analyses also confirmed that the material was not significantly altered by the reprocessing. The Young modulus of Hf-CooAN-10, however, is lower than that of Zr-CooAN-10.

Table 1. Comparison of the Youngs modulus, stress at break and strain at break for Hf-CooAN-10 and Zr-CooAN-10 after each reprocessing cycle.

Material	Cycle	Young mod. (MPa)	Stress at break (MPa)	Strain at break (%)
Hf-CooAN-10	0	2.79 ± 0.43	1.14 ± 0.20	581 ± 49
	1	2.83 ± 0.57	1.24 ± 0.09	485 ± 72
	2	2.33 ± 0.27	1.11 ± 0.18	422 ± 35
	3	2.18 ± 0.32	1.14 ± 0.07	415 ± 61
Zr-CooAN-10[a]	0	6.67 ± 1.83	1.87 ± 0.63	401 ± 175
	1	7.90 ± 1.22	2.56 ± 0.21	486 ± 75
	2	7.57 ± 1.01	2.35 ± 0.16	426 ± 84
	3	6.66 ± 0.65	2.27 ± 0.53	443 ± 59

[a] Values from ref. [6].

[Hf$_6$O$_4$(OH)$_4$(O$_2$CMe)]$_2$/MeCOOH exchange kinetics

Since the exchange mechanism for the reshaping of an adaptable 3D material cannot be unambiguously established from variable-temperature viscosity data,[19] kinetico-mechanistic information was sought from the ligand exchange reaction in a molecular model. The C_{2h}-symmetric [Hf$_6$O$_4$(OH)$_4$(O$_2$CMe)$_{12}$]$_2$ was chosen, because it features both chelating and bridging coordination modes and the corresponding ligands can be distinguished by NMR spectroscopy. The investigations outlined below mirror more or less exactly those recently published by us for the analogous [Zr$_6$O$_4$(OH)$_4$(O$_2$CMe)$_{12}$]$_2$ system.[11]

For each equivalent Hf$_6$ subunit of [Hf$_6$O$_4$(OH)$_4$(O$_2$CMe)$_{12}$]$_2$, the molecular C_{2h} symmetry splits the twelve acetate ligands into seven magnetically inequivalent sets (chelating, 2:1; belt-bridging, 2:2:2; inner-face-bridging, 1; intercluster-bridging, 2) and the four μ$_3$-OH ligands into three sets (1:1:2). The ^{1}H NMR spectra in CD_2Cl_2 and in C_6D_6 (shown in Figure 5) are quite similar to those of the corresponding Zr compound in the same solvents.[11] The spectrum of the Hf$_{12}$ compound in CD_2Cl_2 has also been described in a previous contribution,[7d] though without the identification of the μ$_3$-OH resonances, while the spectrum in C_6D_6 is reported here for the first time. The resonance assignments are based on those previously made for the Zr analogue and are backed up by variable-temperature, DOSY and EXSY NMR analyses, as shown below.

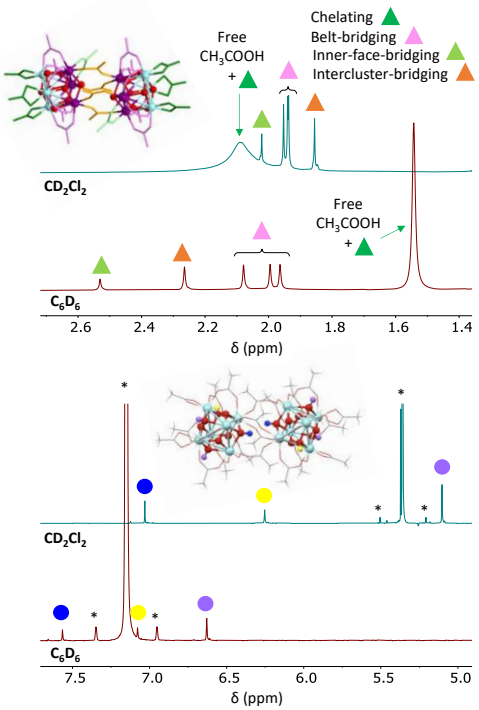

Figure 5. ^{1}H NMR spectra of [Hf$_6$O$_4$(OH)$_4$(O$_2$CMe)$_{12}$]$_2$ in the acetate Me region (above) and μ$_3$-OH region (below) at 25 °C in CD_2Cl_2 and C_6D_6.

Investigation in CD_2Cl_2: low-temperature dynamics

The acetate Me region of the spectrum in CD_2Cl_2 at 25 °C shows a broad and intense band centered at δ 2.09, plus five additional sharp resonances for nine acetate ligands (total of 27H) at δ 2.021, 1.953, 1.940,1.937 and 1.855 in a relative 1:2:2:2:2 ratio. The broad resonance contains the three chelating acetates ligands (9H) and free CH_3COOH (35.9 H, corresponding to ca. 12 molecules) in rapid exchange. Indeed, this resonance decoalesces into two separate resonances when cooling down to -45 °C (Figure 6). At the lowest temperature, this spectrum did not show evidence of any further splitting of the chelating ligand resonance into the expected two bands (2:1 relative intensities), as required by the compound symmetry, whereas a visible shoulder appeared in the spectrum of the Zr_{12} analogue under the same conditions.[11] The assignment of the more intense band observed at δ 2.10 at -45 °C to free MeCOOH is confirmed by the greater diffusion coefficient of this resonance in the DOSY NMR spectrum, recorded also at -45 °C ($D = 7.6 \cdot 10^{-10}$ m^2 s^{-1}, Figure S9), whereas all other resonances have the same lower D value ($2.4 \cdot 10^{-10}$ m^2 s^{-1}). These diffusion coefficients are greater than the corresponding ones measured for free acetic acid and $[Zr_6O_4(OH)_4(O_2CMe)_{12}]_2$ in the same solvent at -80°C (4.1 and $1.6 \cdot 10^{-10}$ m^2 s^{-1}, respectively),[11] because of the lower CD_2Cl_2 viscosity at the higher temperature. Contrary to the Zr_{12} compound, there is no clearly visible resonance attributable to an additional Hf_6 isomer (Figure 1), suggesting that the Hf complex has a greater preference for the Hf_{12} structure.

Upon cooling, the partially overlapped belt-bridging acetate resonances in the δ 1.95-1.93 region at 25 °C shifted slightly to lower frequencies and further split to yield three well-separated resonances. The intercluster-bridging acetate resonance at δ 1.85 also shifts to lower frequencies upon cooling, whereas the chemical shift of the inner-face acetate resonance (δ 2.02) is relatively temperature insensitive.

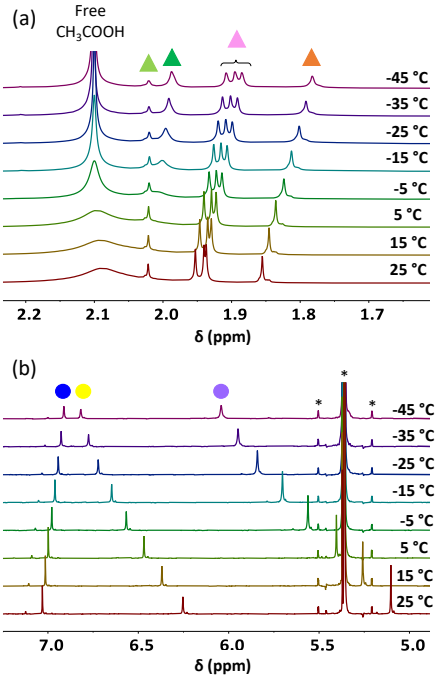

Figure 6. Variable temperature ^{1}H NMR spectra of $[Hf_6O_4(OH)_4(O_2CMe)_{12}]_2$ in CD_2Cl_2 between 25 and -45 °C: (a) acetate Me resonance region; (b) μ_3-OH resonance region. The color coding corresponds to assignments made in Figure 5. The starred resonances belong to the residual $CHDCl_2$ in the deuterated solvent (main resonance and spinning side bands).

The μ_3-OH resonances are observed at 25 °C at δ 7.03 (1H), 6.22 (1H) and 5.07 (2H). The former one slightly shifts to lower frequencies upon cooling, whereas the other two exhibit a much more pronounced shift to higher frequencies. This behavior, which parallels that of the Zr_{12} analogue,[11] is consistent with entropically favored intermolecular H-bonding interactions at lower temperatures for the three externally exposed OH ligands with the free MeCOOH molecules, and allows the assignment of the less temperature-sensitive resonance (δ 7.03 at 25 °C) to the inner μ_3-OH ligand, which is intramolecularly H-bonded to an intercluster-bridging acetate ligand (see Figure 2). The OH resonance of the free acetic acid could not be detected, presumably because it is too broad under these conditions.

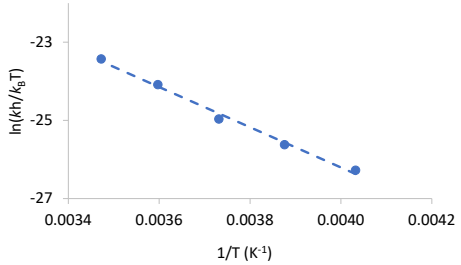

Figure 7. Eyring plot of the temperature-dependent rate coefficient for the exchange of the chelating acetate ligands in the $[Hf_6O_4(OH)_4(O_2CMe)_{12}]_2$ molecule with free acetic acid in CD_2Cl_2.

Table 2. Comparison of the activation parameters for the chelating and belt-bridging acetate ligands in the $[M_6O_4(OH)_4(O_2CMe)_{12}]_2$ compounds (M = Zr, Hf).

Ligand type		Hafnium		Zirconium[a]	
		$\Delta H^{\ddagger}$ (kcal mol^{-1})	$\Delta S^{\ddagger}$ (cal mol^{-1} K^{-1})	$\Delta H^{\ddagger}$ (kcal mol^{-1})	$\Delta S^{\ddagger}$ (cal mol^{-1} K^{-1})
Chelating[b]		10.2±0.5	-11±2	15.0 ± 0.4	8 ± 1
Belt-bridging[c]	1	17.2±1.6	-5±5	22.7±1.6	13±5
	2	23.5±0.8	14±2	22.9±2.1	14±6
	3	20.0±1.1	4±3	20.6±1.0	9±3

[a] Values from ref. [11]. [b] Determined from the low-T investigation in CD_2Cl_2. [c] Determined from the high-T investigation in C_6D_6.

The rate law of the chelating ligand exchange can be determined by observing the effect of a variable free acetic acid concentration on the chelating resonance lineshape. Initial attempts to obtain this information at -5 °C (closer to decoalescence) did not allow a proper lineshape simulation for the spectra with large MeCOOH excess. At -15 °C, on the other hand, the resonance is still significantly broadened relative to the slow exchange limit and allowed proper lineshape simulations (Figure S10) to yield a relatively concentration-independent width, see Figure S11 (average $w_{1/2}$ = 10.3±0.8 Hz, *vs.* $w_{1/2}$ = 7.4 at -25 °C and 5.4 at -35 °C). This establishes a zero-order dependence on $[CH_3COOH]$ for the exchange rate, as previously found also the Zr_{12} analogue. Thus, the pseudo-first order rate coefficient resulting from the lineshape analysis is the true (first-order) rate coefficient. The Eyring analysis of the rate coefficients obtained at the different temperatures (Table S3, simulations shown in Figure S12) was restricted to the values in the -25 to +25 °C range, because the linewidth is highly affected from the viscosity increase at the lowest temperatures, as can be assessed from Figure 6 by the increased linewidth of the non-exchanging

bridging ligand resonances. This analysis (Figure 7) yielded the values reported in Table 2, in comparison with those of the Zr_{12} analogue. The activation enthalpy is lower and the activation entropy is small and negative for the Hf_{12} compound, whereas the Zr_{12} system features a higher $\Delta H^{\ddagger}$ and a small and positive $\Delta S^{\ddagger}$.

Investigation in C_6D_6: high-temperature dynamics

The overall shape of the ^{1}H NMR spectrum in this solvent (Figure 5) is also quite similar to that of the corresponding Zr_{12} compound.[11] Relative to the spectrum in CD_2Cl_2, the acetate Me resonances are spread over a larger chemical shift range and appear in a different relative order, with the resonance of the rapidly exchanging chelating acetates and free MeCOOH at a lower frequency (δ 1.54), followed at increasing frequencies by the belt-bridging acetates (δ 1.96, 1.99 and 2.08), the intercluster-bridging acetates (δ 2.27) and the inner-face-bridging acetate (δ 2.53). The μ_3-OH ligands are in a narrower range and follow the same relative order (δ 6.32 and 7.08 in a 2:1 ratio for the externally exposed ligands and δ 7.56, relative intensity 1, for the inner μ_3-OH ligand). These assignments are comforted by the observed behavior at variable temperature (Figure 8). In the acetate Me region, Figure 8a, the inner-face-bridging and intercluster-bridging resonances shift to lower frequencies but do not change linewidth, whereas the resonances of the belt-bridging acetates (also shifting to lower frequencies) and the already coalesced one for the chelating acetates and free MeCOOH (shifting to higher frequencies) significantly broaden as the temperature increases, suggesting the onset of chemical exchange, as previously witnessed for the Zr_{12} analogue.[11]

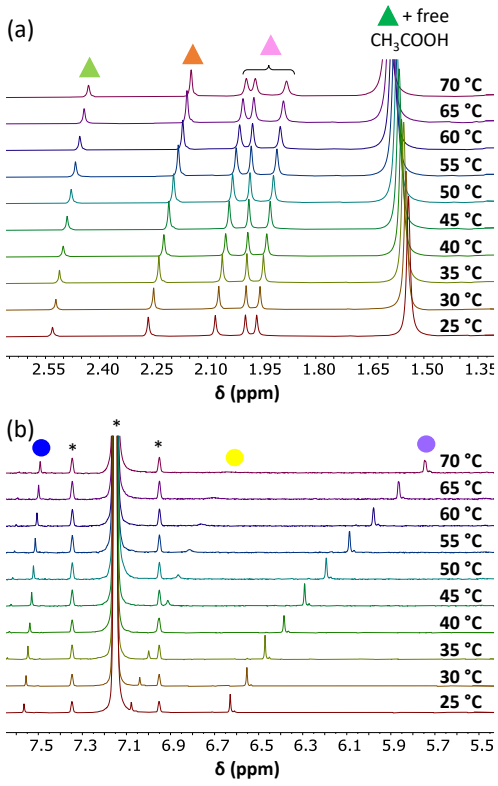

Figure 8. Variable temperature ^{1}H NMR spectra of $[Hf_6O_4(OH)_4(O_2CMe)_{12}]_2$ in C_6D_6 between 25 and 65 °C: (a) acetate Me resonance region; (b) μ_3-OH resonance region. The color coding corresponds to assignments made in Figure 5. The starred resonances belong to the residual C_6HD_5 in the deuterated solvent (main resonance and spinning side bands).

The rate law for the exchange of the belt-bridging ligands was probed, like for the chelating ligands, by measuring the linewidth of the exchanging resonances, at a temperature where the resonances are broadened by the chemical exchange (60 °C), in the presence of a variable excess of MeCOOH (Figure S13). As shown in Figure S14, the linewidths of all three resonances remain essentially constant upon addition of up to 25 equivalents of MeCOOH per Hf_{12} molecule, suggesting once again a zero-order dependence on [MeCOOH]. Hence, the rate-determining step of the exchange does not involve the external acid addition. The linewidths measured as a function of temperature (Figure S15) confirm that the three belt-bridging acetate resonances start to broaden at temperatures > 40 °C, whereas the other bridging acetate resonances maintain a constant linewidth (Figure S16). The widths of the belt-bridging resonances were used to extract the exchange rate coefficients (Table S4). Of these, the Eyring analyses over the 55-70 °C temperature range (Figure 9) gave the activation parameters reported in Table 2, in comparison with those of the Zr_{12} analogue. The data at lower temperatures are too close to the slow exchange limit (see Figure S16) and are thus affected by too large errors. Overall, the behavior of the Zr_{12} and Hf_{12} compounds is quite comparable: exchange rate laws with zero-order dependence on [MeCOOH] for both chelating and belt-bridging acetates, faster exchange for the chelating acetates (lower $\Delta H^{\ddagger}$) and low $\Delta S^{\ddagger}$ values. The latter seem smaller in the Hf_{12} compound, particularly for certain resonances, though the large standard deviations and the limited temperature range of the investigations call for caution in this comparison.

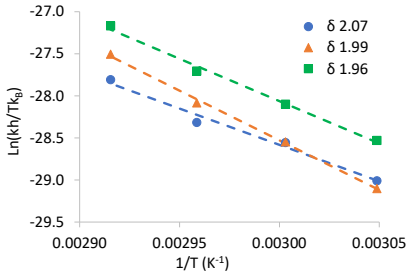

Figure 9. Eyring plot of the temperature-dependent rate coefficients for the exchange of the belt-bridging acetate ligands in the $[Hf_6O_4(OH)_4(O_2CMe)_{12}]_2$ molecule with free acetic acid in C_6D_6.

The μ_3-OH resonances, Figure 8b, exhibit the same behavior as in the lower-temperature range in CD_2Cl_2: the two lower frequency resonances of the outer ligands continue to move to lower frequencies as the temperature increases, while that assigned to the inner ligand is relatively temperature-independent. A significant broadening occurs for the outer μ_3-OH resonance of relatively intensity 1. For the corresponding Zr_{12} molecule, the same resonance in C_6D_6 was found to split into two resonances at high temperatures, globally worth 1H and with temperature-dependent relative intensities. For both metal complexes, this behavior can be rationalized on the basis of the presence of a thermally populated second species, which may be postulated (on the basis of the DFT investigation, *vide infra*) to be the associative intermediate of acetate exchange, as shown in Scheme 3. For the Zr_{12} compound, the two species in equilibrium are very close in relative energy and exchange slowly, thus allowing the individual resonances to be observed.[11] In the Hf_{12} case, on the other hand,

the line broadening indicates faster exchange, but the intermediate must be at significantly higher energy because it is not significantly populated in the slow exchange regime (< 40°C). Splitting (for Zr_{12}) or broadening (for Hf_{12}) is only observed for the resonance of the magnetically unique outer μ_3-OH ligand, suggesting that the most accessible associative intermediate involves this particular ligand, but does not exclude the involvement of the other μ_3-OH ligands in analogous kinetically competent intermediates.

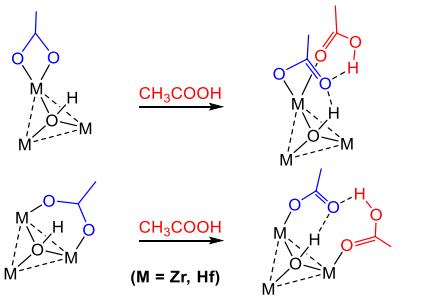

Scheme 3. Possible thermally populated intermediates of the exchange processes of (a) chelating acetate and (b) belt-bridging acetate.

DFT investigation of the ligand exchange mechanism

The previous investigation on the Zr system,[11] conducted on the $[Zr(O_2CMe)_2(\mu\text{-}O_2CMe)(OH)(H_2O)]_2$ model compound, has revealed an initial and rate-limiting partial dissociation of the outgoing (chelating or bridging) acetate, with the dissociating carbonyl O donor shifting to the OH ligand. Namely, the O-Zr dative bond is broken and an O···H hydrogen-bond is simultaneously formed. The subsequent acetic acid coordination and the symmetric proton transfer, which transforms the outgoing acetate to a coordinated acetic acid and *vice versa*, were shown to be rapid, in agreement with the zero-order dependence of the rate law on [MeCOOH]. On the basis of these previous results, the DFT investigation on the Hf system was limited to the rate-limiting partial dissociation step.

The chosen computational model, dinuclear $[Hf(O_2CMe)_2(\mu\text{-}O_2CMe)(OH)(H_2O)]_2$, is identical to that used for the corresponding Zr study and is related to a series of tetracarboxylate dimers, $[Hf(O_2CR)_2(\mu\text{-}O_2CR)_2]_2$ (R = *i*Pr, *t*Bu, Np),[20] where each metal atom is coordinated by two chelating carboxylate ligands and the two metal atoms are bridged by four carboxylates (Figure 10). In order to properly account for the H-bonding assistance by the OH ligand that caps the belt triangular face (Scheme 3), one bridging acetate per Hf atom was replaced by the electronically equivalent $(OH)(H_2O)$ combination. Two different orientations of the OH ligand (*anti* and *syn* with respect to the two bridging acetates) were necessary to provide the most favorable pathways for the exchange of both chelating and bridging acetates, respectively, see Figure 10. The dissociating carbonyl of the bridging acetate can only dock onto the *syn*-OH ligand, whereas the carbonyl group of the dissociated chelating acetate could equally well use the *syn* and *anti*-OH ligands, but the latter has a slightly lower energy (Figure 11).

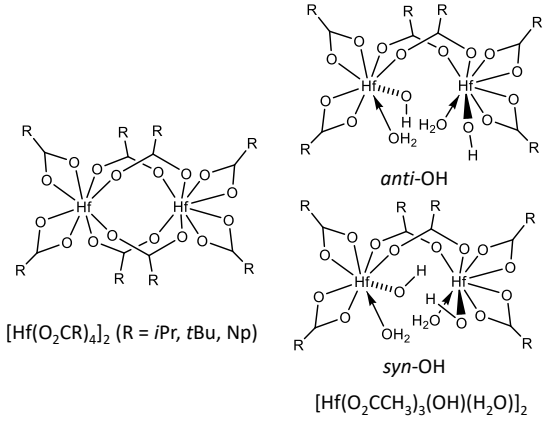

Figure 10. Geometries of the $[Hf(O_2CR)_2(\mu\text{-}O_2CR)_2]_2$ (R = *i*Pr, *t*Bu, Np) molecules[20] (left) and of the $[Hf(O_2CMe)_2(\mu\text{-}O_2CMe)(OH)(H_2O)]_2$ models used for the DFT calculations (right).

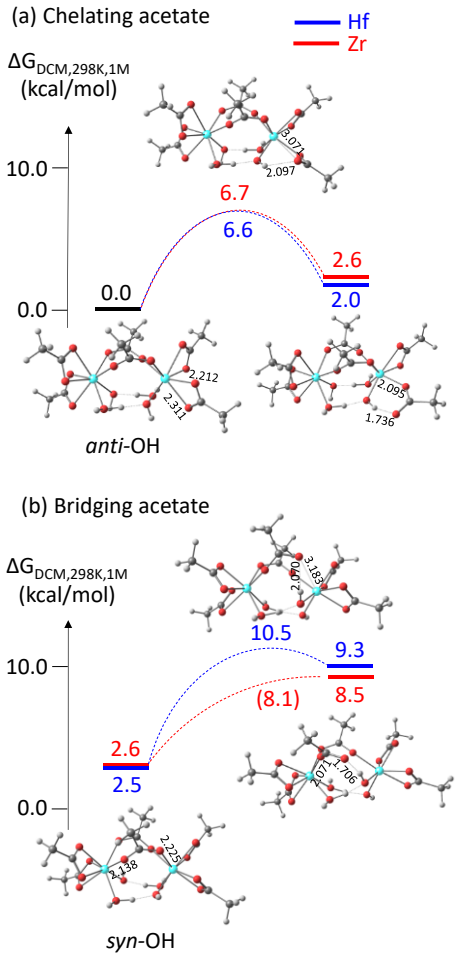

Figure 11. Comparative Gibbs energy profiles for the partial dissociation of (a) a chelating and (b) a bridging acetate ligand in $[M(O_2CMe)_2(\mu\text{-}O_2CMe)(OH)(H_2O)]_2$ (M = Zr, blue lines; Hf, red lines).

For the dissociation of a chelating acetate ligand (Figure 11a) both the activation barrier ($\Delta G^{\ddagger}$ = 6.6 kcal mol^{-1}) and the relative energy of the C=O···H-O intermediate (ΔG = 2.0 kcal mol^{-1}) are very similar for the two metal systems. The release of ring strain

for the 4-membered chelate ring contributes to the relative stabilization of the intermediate. A finer analysis of the activation barriers indicates enthalpic and entropic components of $\Delta H^{\ddagger}$ = 5.7 kcal mol^{-1} and $\Delta S^{\ddagger}$ = -4.5 cal mol^{-1} K^{-1} for Hf and $\Delta H^{\ddagger}$ = 4.9 kcal mol^{-1} and $\Delta S^{\ddagger}$ = -6.0 cal mol^{-1} K^{-1} for Zr. Inspection of the key distances (Figure S17) shows slightly shorter M-O distances for Hf, both in the starting material and in the transition state, whereas the O···H distance is longer in the Hf system, both in the TS and intermediate complex.

The barrier for the bridging acetate opening, with assistance by the *syn*-OH ligand (Figure 11b), is higher than the chelating acetate opening barrier, consistent with the experimental result. In this case, the bridge opening also has a higher thermodynamic cost, similar for both metals. The calculated barrier is in this case slightly greater for the Hf system ($\Delta G^{\ddagger}$ = 10.5 kcal mol^{-1}). Note that, based on the optimized Hf geometry, the TS for the Zr system was reoptimized and found to yield a slightly lower G geometry relative to that reported in the previous contribution.[11] The enthalpic and entropic components are $\Delta H^{\ddagger}$ = 10.7 kcal mol^{-1} and $\Delta S^{\ddagger}$ = 1.0 cal mol^{-1} K^{-1} for Hf and $\Delta H^{\ddagger}$ = 6.5 kcal mol^{-1} and $\Delta S^{\ddagger}$ = -5.6 cal mol^{-1} K^{-1} for Zr.

The absolute values and trends obtained from the DFT calculations do not completely match those obtained from the experiments (Table 2). Notably, the calculated $\Delta H^{\ddagger}$ values are much smaller than the experimental values. These discrepancies may be attributed to a non-ideal level of the calculations (*e.g.* functional/basis sets/corrections) and to the non-ideal truncation of the real molecules. In particular, the OH ligand used for docking the dissociated carbonyl group in H-bonding is bound in a terminal mode in the model molecule, whereas it is triply bridging in the real system. Wider explorations with other computational methods and molecular models are beyond the scope of this investigations. The computational results, however, have captured the essential points of the kinetic investigations and provide a satisfactory rationalization of the exchange mechanism: (*i*) the exchange of the chelating acetates has a lower barrier than the exchange of the bridging ones; (*ii*) the rate-determining step does not involve the free CH_3COOH reagent; (*iii*) the optimized geometries of the rate-determining transition states are consistent with small activation entropies; (*iv*) the barriers for the Hf system are similar to those of the Zr analogue.

Conclusion

The present contribution has introduced Hf-CooAN-10, the first coordination adaptable network based on hafnium as the metal in the crosslinking unit. The crosslink migration is based on the exchange of carboxylate ligands with free carboxylic acid functions. The material has the same chemical constitution and metal loading (10% molar) and was assembled by the same method as the recently disclosed material based on zirconium. The physico-chemical and rheological properties of the Zr and Hf CooAN-10 materials are also very similar. Given the higher cost of hafnium, using Hf-based coordination vitrimers for mechanical applications is thus unjustified. However, such materials may have an interest for applications based on the specific properties of Hf. The molecular compounds used as models for the kinetico-mechanistic ligand exchange studies ($[M_6O_4(OH)_4(O_2CMe)_{12}]_2$/MeCOOH; M = Zr, Hf) reveal minor differences of the activation parameters, but the exchange mechanism is the same for both metals, with rate-determining partial dissociation of the acetate ligand followed by associative exchange. Extrapolation of this mechanism to the Hf-CooAN-10 material qualifies the latter as a coordination vitrimer. The exchange reaction of carboxylate ligands with free carboxylic acids is a ubiquitous reaction in coordination chemistry and several mono- and polynuclear complexes containing more than two carboxylate ligands exist for a variety of metals. Therefore, the development of a rich and tunable family of M-CooAN materials differing by the metal nature, crosslink structure, and polymer matrix properties can be envisaged for a myriad of different applications.

Experimental Section

Materials. $Hf(O^tBu)_4$ (99.9%) was purchased from abcr and used as received. Acetic acid, toulene, dichloromethane, ethanol and dimethlformamide were purchased from Carlo Erba and were used without further purification except CH_2Cl_2, which was dehydrated over CaH_2 and distilled under Ar when used for the synthesis of the Hf starting material. C_6D_6 and CD_2Cl_2 were purchased from Sigma -Aldrich and used without further purification. Poly-((ethylhexyl methacylate)-*co*-(carboxyethyl acrylate)) (M_n = 14.4 kg mol $^{-1}$, Đ = 2.2) was synthesized by the AIBN-initiated radical copolymerization of the two monomers in a 9:1 ratio as described in the literature.[15] The $[Hf_6O_4(OH)_4(O_2CMe)_{12}]_2$ compound used for the Hf-CooAN preparation and for the acetate exchange mechanistic investigation was synthesized as described in the literature.[7d] However, the compound was also prepared by a new method (see below). The analytical instrumentation is descrined in the SI (section S1).

Synthesis of $[Hf_6O_4(OH)_4(O_2CMe)_{12}]_2$·4MeCOOH·4HCOOH. $HfOCl_2.8H_2O$ (0.737 g, 1.80 mmol) was dissolved in a mixture of DMF (0.9 mL) and acetic acid (3.975 mL) in a round bottom flask. The resulting homogeneous solution was kept at 110 °C without stirring for 24 h. White crystals of the product appeared after the reaction was cooled to room temperature (0.491 g, 77.0 %).

Synthesis of the Hf-CooAN-10 material. Poly-((ethylhexyl methacylate)-co-(carboxyethyl acrylate)) (10 g, 5.18 mmol of COOH groups) was dissolved in CH_2Cl_2 (50 mL). In a separate container, a solution containing $[Hf_6O_4(OH)_4(O_2CMe)_{12}]_2$·6MeCOOH·3.5$CH_2Cl_2$ (123.86 mg, 0.0648 mmol) in a mixture of ethanol (20 mL) and CH_2Cl_2 (20 mL) was prepared. Then, the two solutions were mixed with stirring in a Teflon mold. The resulting homogeneous solution was cured overnight at 70 °C in a hot-air oven to obtain the Hf-CooAN-10-Pre intermediate. This material was subsequently kept in a vacuum oven at 120°C for 72 h to obtain Hf-CooAN-10. For the determination of the swelling ratio and insoluble fraction, a Teflon bag containing ca. 20 mg of the sample was immersed in THF for 24 h at room temperature, then retrieved and the excess solvent on the bag surface was wiped off with a paper tissue. The swelling ratio is the weight ratio of swollen and initial sample. The recovered sample was then dried for 24 h in a vacuum oven at 70°C. The insoluble fraction is the weight fraction of dried and initial sample. The reported values are averages and standard deviations of the results of 3 separate measurements.

X-ray structural determination. A single crystal of compound was mounted under inert perfluoropolyether at the tip of glass fiber and cooled in the cryostream of a Bruker APEX II CCD diffractometer using a microfocus sealed tube. The structure was solved by using the integrate space-group and crystal structure determination SHELXT[21] software and refined by least-squares procedures on F2 using SHELXL-2014.[22] All H atoms attached to carbon were introduced in calculation in idealised positions and treated as riding models. The H atoms attached to oxygen were localized on difference Fourier synthesis and their coordinates and Uiso refined

using restraints. Besides the Hf complex, the asymmetric unit revealed the presence of one formic acid and two acetic acid molecules. One of these two acetic acid molecules is disordered by rotation around one of the C-O bond (C301-O300, see Figure S1), the oxygen atom of which is hydrogen-bonded to one of the triply bridging OH ligands. This structure is isomorphous with that of the corresponding Zr compound ($P2_1/c$, a = 20.287(3) Å, b = 12.5914(18) Å, c = 20.241(3) Å, $\alpha = \gamma = 90°$, β = 100.188(2)°, V = 5088.9(13) Å^3.[16] However, whereas the latter was described as $[Zr_{12}O_8(OH)_8(O_2CMe)_{24}]\cdot 4MeCOOH\cdot 2HCOOH\cdot 0.5H_2O$, no interstitial water molecule could be found in the present structure. The drawing of the molecules was realised with the help of ORTEP32.[23] Crystal data and refinement parameters are collected in Table S1 and selected bond distances are listed in Table S2. Deposition Number <url href="https://www.ccdc.cam.ac.uk/services/structures?id=doi:10.1002/ejic.202300672">2297364</url> contains the supplementary crystallographic data for this paper. These data are provided free of charge by the joint Cambridge Crystallographic Data Centre and Fachinformationszentrum Karlsruhe <url href="http://www.ccdc.cam.ac.uk/structures">Access Structures service</url>.

Computational details. The calculations made use of the Gaussian09 suite of programs.[24] Geometry optimizations were carried out without any symmetry constraint using the B3LYP functional, the 6-31G(d,p) basis functions for all light atoms (H, C, O) and the SDD basis set augmented by an f polarisation function (α = 0.784) for the Hf atom.[25] The effects of dispersion forces and of solvation effects were considered by using a polarizable continuum (SMD[26] in CH_2Cl_2) and Grimme's D3 empirical method[27] during the optimization process. The thermal corrections leading to the Gibbs energy (zero-point vibrational energy or ZPVE, PV, and TS) were obtained from the solution of the nuclear equation using the standard ideal gas and harmonic approximations at T = 298.15 K (25 °C), which also verified the nature of all optimized geometries as local minima or first-order saddle points. A correction of 1.95 kcal/mol was applied to all G values to change the standard state from the gas phase (1 atm) to solution (1 M).[28]

Supporting Information

The authors have cited additional references within the Supporting Information.

Acknowledgements

The French National Research Agency (ANR) is gratefully acknowledged for funding this research (AFCAN program, ANR-19-CE06-0014). RP is grateful to the CALMIP mesocenter of the University of Toulouse for the allocation of computational resources.

Keywords: Hafnium • coordination adaptable networks • carboxylate exchange • rheology • vitrimers

[1] a) C. J. Kloxin, T. F. Scott, B. J. Adzima, C. N. Bowman, *Macromolecules* **2010**, *43*, 2643-2653; b) C. J. Kloxin, C. N. Bowman, *Chem. Soc. Rev.* **2013**, *42*, 7161-7173; c) G. M. Scheutz, J. J. Lessard, M. B. Sims, B. S. Sumerlin, *J. Am. Chem. Soc.* **2019**, *141*, 16181-16196.
[2] D. Montarnal, M. Capelot, F. Tournilhac, L. Leibler, *Science* **2011**, *334*, 965-968.
[3] a) W. Denissen, J. M. Winne, F. E. Du Prez, *Chem. Sci.* **2016**, *7*, 30-38; b) M. Guerre, C. Taplan, J. M. Winne, F. E. Du Prez, *Chem. Sci.* **2020**, *11*, 4855-4870; c) B. Krishnakumar, R. Sanka, W. H. Binder, V. Parthasarthy, S. Rana, N. Karak, *Chem. Eng. J.* **2020**, *385*, 12382; d) M. A. Lucherelli, A. Duval, L. Averous, *Progr. Polym. Sci.* **2022**, *127*.
[4] a) B. Sandmann, S. Bode, M. D. Hager, U. S. Schubert, *Adv. Polym. Sci.* **2013**, *262*, 239-257; b) M. Enke, D. Dohler, S. Bode, W. H. Binder, M. D. Hager, U. S. Schubert, *Adv. Polym. Sci.* **2016**, *273*, 59-112; c) H. Li, P. Yang, P. Pageni, C. B. Tang, *Macromol. Rapid Comm.* **2017**, *38*; d) G. I. Dzhardimatieva, B. C. Yadav, S. Singh, I. E. Uflyand, *Dalton Trans.* **2020**, *49*, 3042-3087; e) C.-H. Li, J.-L. Zuo, *Advanced Materials* **2020**, *32*, 1903762; f) S. Basak, A. Bandyopadhyay, *J. Organomet. Chem.* **2021**, *956*; g) S. Gotz, S. Zechel, M. D. Hager, G. R. Newkome, U. S. Schubert, *Progr. Polym. Sci.* **2021**, *119*, 101428.
[5] M. Murali, E. Manoury, R. Poli, *Eur. J. Inorg. Chem.* **2023**, *26*, e202300574.
[6] M. Murali, D. Berne, C. Joly-Duhamel, S. Caillol, E. Leclerc, E. Manoury, V. Ladmiral, R. Poli, *Chem. Eur. J.* **2022**, *28*, e202202058.
[7] a) G. Kickelbick, P. Wiede, U. Schubert, *Inorg. Chim. Acta* **1999**, *284*, 1-7; b) G. Kickelbick, U. Schubert, *Chem. Ber.* **1997**, *130*, 473-477; c) C. Hennig, S. Weiss, W. Kraus, J. Kretzschmar, A. C. Scheinost, *Inorg. Chem.* **2017**, *56*, 2473-2480; d) M. Puchberger, F. R. Kogler, M. Jupa, S. Gross, H. Fric, G. Kickelbick, U. Schubert, *Eur. J. Inorg. Chem.* **2006**, 3283-3293.
[8] a) J. H. Cavka, S. Jakobsen, U. Olsbye, N. Guillou, C. Lamberti, S. Bordiga, K. P. Lillerud, *J. Am. Chem. Soc.* **2008**, *130*, 13850-13851; b) F. Vermoortele, R. Ameloot, A. Vimont, C. Serre, D. De Vos, *Chem. Commun.* **2011**, *47*, 1521-1523; c) S. Waitschat, D. Frohlich, H. Reinsch, H. Terraschke, K. A. Lomachenko, C. Lamberti, H. Kummer, T. Helling, M. Baumgartner, S. Henningerb, N. Stock, *Dalton Trans.* **2018**, *47*, 1062-1070; d) M. Kandiah, M. H. Nilsen, S. Usseglio, S. Jakobsen, U. Olsbye, M. Tilset, C. Larabi, E. A. Quadrelli, F. Bonino, K. P. Lillerud, *Chem. Mater.* **2010**, *22*, 6632-6640; e) S. J. Garibay, S. M. Cohen, *Chem. Commun.* **2010**, *46*, 7700-7702; f) M. L. Foo, S. Horike, T. Fukushima, Y. Hijikata, Y. Kubota, M. Takata, S. Kitagawa, *Dalton Trans.* **2012**, *41*, 13791-13794; g) M. J. Katz, Z. J. Brown, Y. J. Colon, P. W. Siu, K. A. Scheidt, R. Q. Snurr, J. T. Hupp, O. K. Farha, *Chem. Commun.* **2013**, *49*, 9449-9451; h) S. Biswas, J. Zhang, Z. B. Li, Y. Y. Liu, M. Grzywa, L. X. Sun, D. Volkmer, P. Van der Voort, *Dalton Trans.* **2013**, *42*, 4730-4737; i) K. K. Yee, N. Reimer, J. Liu, S. Y. Cheng, S. M. Yiu, J. Weber, N. Stock, Z. T. Xu, *J. Am. Chem. Soc.* **2013**, *135*, 7795-7798; j) T. Ntep, H. Reinsch, B. Moll, E. Hasturk, S. Goekpinar, H. Breitzke, C. Schlusener, L. Schmolke, G. Buntkowsky, C. Janiak, *Chem. Eur. J.* **2018**, *24*, 14048-14053.
[9] D. Van den Eynden, R. Pokratath, J. P. Mathew, E. Goossens, K. De Buysser, J. De Roo, *Chem. Sci.* **2023**, *14*, 573-585.
[10] a) J. Kreutzer, M. Puchberger, C. Artner, U. Schubert, *Eur. J. Inorg. Chem.* **2015**, 2145-2151; b) F. R. Kogler, M. Jupa, M. Puchberger, U. Schubert, *J. Mater. Chem.* **2004**, *14*, 3133-3138.
[11] M. Murali, C. Bijani, J.-C. Daran, E. Manoury, R. Poli, *Chem. Sci.* **2023**, *14*, 8152–8163.
[12] J. A. Sommers, L. Palys, N. P. Martin, D. B. Fast, M. Amiri, M. Nyman, *J. Am. Chem. Soc.* **2022**, *144*, 2816-2824.
[13] a) S. Gross, G. Kickelbick, M. Puchberger, U. Schubert, *Monatsh. Chem.* **2003**, *134*, 1053-1063; b) F. Faccini, H. Fric, U. Schubert, E. Wendel, O. Tsetsgee, K. Mueller, H. Bertagnolli, A. Venzo, S. Gross, *J. Mater. Chem.* **2007**, *17*, 3297-3307.
[14] a) S. Jakobsen, D. Gianolio, D. S. Wragg, M. H. Nilsen, H. Emerich, S. Bordiga, C. Lamberti, U. Olsbye, M. Tilset, K. P. Lillerud, *Physical Review B* **2012**, *86*, 125429; b) P. Xydias, I. Spanopoulos, E. Klontzas, G. E. Froudakis, P. N. Trikalitis, *Inorg. Chem.* **2014**, *53*, 679-681; c) Z. G. Hu, A. Nalaparaju, Y. W. Peng, J. W. Jiang, D. Zhao, *Inorg. Chem.* **2016**, *55*, 1134-1141; d) Z. G. Hu, I. Castano, S. N. Wang, Y. X. Wang, Y. W. Peng, Y. H. Qan, C. L. Chi, X. R. Wang, D. Zhao, *Crystal Growth & Design* **2016**, *16*, 2295-2301; e) T. Ntep, H. Reinsch, C. Schlusener, A. Goldman, H. Breitzke, B. Moll, L. Schmolke, G. Buntkowsky, C. Janiak, *Inorg. Chem.* **2019**, *58*, 10965-10973.
[15] Y. Vidavsky, S. Bae, M. N. Silberstein, *J. Polym. Sci., Polym. Chem.* **2018**, *56*, 1117-1122.
[16] A. A. Bezrukov, K. W. Tornroos, E. Le Roux, P. D. C. Dietzel, *Chem. Commun.* **2018**, *54*, 2735-2738.

[17] a) W. Morris, B. Volosskiy, S. Demir, F. Gandara, P. L. McGrier, H. Furukawa, D. Cascio, J. F. Stoddart, O. M. Yaghi, *Inorg. Chem.* **2012**, *51*, 6443-6445; b) J. E. Mondloch, W. Bury, D. Fairen-Jimenez, S. Kwon, E. J. DeMarco, M. H. Weston, A. A. Sarjeant, S. T. Nguyen, P. C. Stair, R. Q. Snurr, O. K. Farha, J. T. Hupp, *J. Am. Chem. Soc.* **2013**, *135*, 10294-10297; c) H. Reinsch, I. Stassen, B. Bueken, A. Lieb, R. Ameloot, D. De Vos, *CrystEngComm* **2015**, *17*, 331-337; d) M. Lammert, H. Reinsch, C. A. Murray, M. T. Wharmby, H. Terraschke, N. Stock, *Dalton Trans.* **2016**, *45*, 18822-18826.
[18] a) C. Ortiz, C. K. Ober, E. J. Kramer, *Polymer* **1998**, *39*, 3713-3718; b) H. H. Le, T. Lüpke, T. Pham, H. J. Radusch, *Polymer* **2003**, *44*, 4589-4597; c) A. Batra, C. Cohen, L. Archer, *Macromolecules* **2005**, *38*, 7174-7180; d) K. Yamaguchi, A. G. Thomas, J. J. C. Busfield, *International Journal of Non-Linear Mechanics* **2015**, *68*, 66-70; e) L. Imbernon, S. Norvez, L. Leibler, *Macromolecules* **2016**, *49*, 2172-2178; f) S. Qi, M. Yu, J. Fu, M. Zhu, *Journal of Intelligent Material Systems and Structures* **2018**, *29*, 205-213; g) T. Ohzono, K. Katoh, H. Minamikawa, M. O. Saed, E. M. Terentjev, *Nat. Commun.* **2021**, *12*.
[19] N. J. Van Zee, R. Nicolay, *Progr. Polym. Sci.* **2020**, *104*.
[20] T. J. Boyle, D. T. Yonemoto, T. Q. Doan, T. M. Alam, *Inorg. Chem.* **2014**, *53*, 12449-12458.
[21] G. M. Sheldrick, *Acta Crystallogr. A* **2015**, *71*, 3-8.
[22] G. M. Sheldrick, *Acta Crystallogr. C* **2015**, *71*, 3-8.
[23] a) L. J. Farrugia, *J. Appl. Cryst.* **1997**, *30*, 565; b) M. N. Burnett, C. K. Johnson, *ORTEPIII, Report ORNL-6895.* , Oak Ridge National Laboratory, Oak Ridge, Tennessee, U.S. , **1996**, p.
[24] M. J. Frisch, G. W. Trucks, H. B. Schlegel, G. E. Scuseria, M. A. Robb, J. R. Cheeseman, G. Scalmani, V. Barone, G. A. Petersson, H. Nakatsuji, X. Li, M. Caricato, A. V. Marenich, J. Bloino, B. G. Janesko, R. Gomperts, B. Mennucci, H. P. Hratchian, J. V. Ortiz, A. F. Izmaylov, J. L. Sonnenberg, D. Williams-Young, F. Ding, F. Lipparini, F. Egidi, J. Goings, B. Peng, A. Petrone, T. Henderson, D. Ranasinghe, V. G. Zakrzewski, J. Gao, N. Rega, G. Zheng, W. Liang, M. Hada, M. Ehara, K. Toyota, R. Fukuda, J. Hasegawa, M. Ishida, T. Nakajima, Y. Honda, O. Kitao, H. Nakai, T. Vreven, K. Throssell, J. A. Montgomery Jr., J. E. Peralta, F. Ogliaro, M. J. Bearpark, J. J. Heyd, E. N. Brothers, K. N. Kudin, V. N. Staroverov, T. A. Keith, R. Kobayashi, J. Normand, K. Raghavachari, A. P. Rendell, J. C. Burant, S. S. Iyengar, J. Tomasi, M. Cossi, J. M. Millam, M. Klene, C. Adamo, R. Cammi, J. W. Ochterski, R. L. Martin, K. Morokuma, O. Farkas, J. B. Foresman, D. J. Fox, *Gaussian 16, Revision C.01*, Gaussian, Inc., Wallingford CT, **2016**, p.
[25] A. W. Ehlers, M. Böhme, S. Dapprich, A. Gobbi, A. Hoellwarth, V. Jonas, K. F. Koehler, R. Stegmann, A. Veldkamp, G. Frenking, *Chem. Phys. Lett.* **1993**, *208*, 111-114.
[26] A. V. Marenich, C. J. Cramer, D. G. Truhlar, *J. Phys. Chem. B* **2009**, *113*, 6378-6396.
[27] S. Grimme, J. Antony, S. Ehrlich, H. Krieg, *J. Chem. Phys.* **2010**, *132*, 154104.
[28] V. S. Bryantsev, M. S. Diallo, W. A. Goddard, III, *J. Phys. Chem. B* **2008**, *112*, 9709-9719.

Entry for the Table of Contents

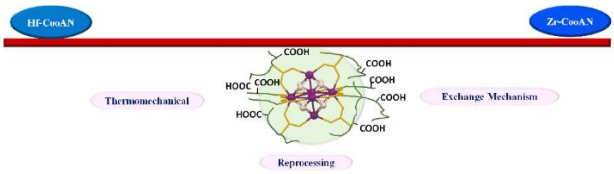

The contribution reports the first hafnium-based coordination adaptable network (Hf-CooAn-10), based on carboxylate/carboxylic acid exchange, and kinetico-mechanistic studies of the exchange in the molecular $[Hf_6O_4(OH)_4(O_2CMe)_{12}]_2$/MeCOOH model system, which demonstrates the operationally associative exchange and qualifies the material as a coordination vitrimer.

Institute and/or researcher Twitter usernames: @lcc_cnrs